Fast-Frequency Response Provided by DFIG-Wind Turbines and its Impact on the Grid

Danny Ochoa, *Member, IEEE*, and Sergio Martinez, *Member, IEEE*

***Abstract*—This paper presents a methodology for the analysis of frequency dynamics in large-scale power systems with high level of wind energy penetration by means of a simplified model for DFIG-based wind turbines. In addition, a virtual inertia controller version of the optimized power point tracking (OPPT) method is implemented for this kind of wind turbines, where the maximum power point tracking curve is shifted to drive variations in the active power injection as a function of both the grid frequency deviation and its time derivative. The proposed methodology integrates the model in a primary frequency control scheme to analyze the interaction with the rest of the plants in the power system. It is also proven that, under real wind conditions, the proposed version of the OPPT method allows us to smooth the wind power injected into the grid, thereby reducing frequency fluctuations.**

***Index Terms*—Ancillary services, doubly-fed induction generator, fast-frequency response, primary frequency control, wind power integration.**

I. Introduction

THE rapid increase in the penetration of wind power plants in power systems has resulted in significant advances in wind turbine (WT) technology. At the same time, the need of integration of higher penetration levels has led power system operators to set new requirements to WT, such as having low voltage ride-through capability or being able to provide ancillary services, to transform them into grid-friendly power generation sources [1].

A major concern in the operation of power systems with a high share of wind power is the frequency stability, particularly when a period with high wind production coincides with a reduced demand. In such a condition many conventional power plants may be forced offline, thus resulting in the loss of inertia from their rotating masses [1]. This situation may be worse in isolated power systems [2], [3].

From the available technologies for wind generation, this work is focused on the doubly-fed induction generator based wind turbine (DFIG-WT) because it has attained most of the market share in the last decade [4]–[6]. Given the operational characteristics of this type of WT, it would seem it cannot compete with conventional generation in offering certain ancillary services, specifically those related to the primary frequency control, as they are heavily limited by the intermittent nature of wind. In addition, modern WTs lack from natural inertia response due to the decoupling between rotor speed and grid frequency. However, in recent years, various studies have shown that it is possible to act on the sophisticated control system of a WT to provide a wide range of ancillary services [1]. In this context, supplementary control strategies to provide variable speed WTs with an effective inertial response to meet the grid requirements have been developed [7]–[10]. Additionally, references [7], [11], [12] propose several frequency-droop schemes by acting on the blade pitch angle to preserve a power reserve margin for primary frequency regulation. A common aspect in the aforementioned works is the use of detailed WT models that represent quite accurately the behavior of real prototypes. However, its application in multi-machine and large-scale power system studies may be impractical due to the huge computational effort required [13].

Three are the main contributions of this work. First, the paper presents a methodology for analyzing the frequency response of large-scale power systems using a primary frequency control scheme. This scheme includes linearized models of the speed governors of conventional power plants and their inertial characteristics, the frequency sensitivity of the load, and a simplified model of the DFIG-WT, instead of a detailed representation of the grid components that would be intractable when simulating frequency events. Second, the paper proposes an adaptation of the optimized power point tracking (OPPT) method for a Permanent Magnet Synchronous Generator based wind turbine [14] to a DFIG-WT. This method consists in shifting the maximum power point tracking (MPPT) curve to produce variations in the WT active power output as a function of the grid frequency deviation, relying on its available inertial resources. The proposed adaptation includes the ability to operate under real wind conditions and aims to the additional objective of smoothing the power injected into the grid. Third, an extension of the adapted OPPT method is proposed so as to reduce the frequency fluctuations produced by such intermittent energy source and improve the power quality. It is based on including the time derivative of frequency as a new control variable, as in virtual inertia approaches [12], although not directly acting on the active power reference but on the shifting of the MPPT curve.

This paper is organized as follows. In Section II, a simplified electromechanical DFIG-WT model is presented. Section III introduces the concept of virtual inertia and section IV illustrates

Manuscript received July 14, 2016; revised October 20, 2016 and November 30, 2016; accepted December 3, 2016. Date of publication December 7, 2016; date of current version August 17, 2017. This work was supported in part by the SENESCYT, Government of the Republic of Ecuador under Grant 2015-AR6C5141. Paper no. TPWRS-01068-2016.

The authors are with the Department of Electrical Engineering, ETSI Industriales, Universidad Politecnica de Madrid, Madrid 28006, Spain (e-mail: danny.ochoac@alumnos.upm.es; sergio.martinez@upm.es).

Digital Object Identifier 10.1109/TPWRS.2016.2636374

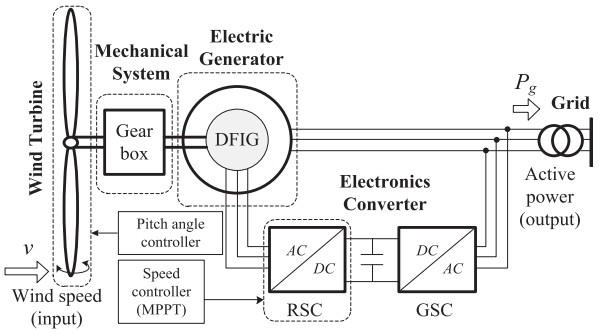

Fig. 1. DFIG-based wind turbine general scheme.

the method that uses that concept to take advantage of the stored kinetic energy in a DFIG-WT. Section V explains the utilization of the developed model in a primary frequency control scheme. Finally, Section VI shows some results that demonstrate the effectiveness of the presented method by means of time domain simulation in MATLAB/Simulink. To allow the reproduction of the cases, the Appendix includes the values assigned to all parameters.

II. Simplified Model of a DFIG-Based Wind Turbine

Fig. 1 shows the main components of a DFIG-WT: wind turbine, gear-box, doubly-fed induction generator (DFIG) and a power electronics converter (PEC). The operating principle of the DFIG is based on injecting three-phase currents of variable amplitude and frequency into the rotor to allow the operation under different rotor speeds to achieve the maximum wind power extraction. The stator is connected directly to the grid to deliver most of the electrical energy produced.

The PEC is composed of two back-to-back electronic units, the rotor side converter (RSC) and the grid side converter (GSC). The objective of the GSC is to regulate the DC-link voltage, the bidirectional flow of active power from the DFIG rotor to the grid, and the injection of reactive power [4]. The RSC is responsible for controlling the optimum production of active power, but it also allows to regulate the reactive power in the DFIG stator [15]. One of the main objectives of the work described in this paper is to provide the DFIG-WT with inertial response by means of a controlled variation of its active power, so the analysis and modeling efforts are focused on the RSC.

Fig. 2 shows the block diagram of the simplified electromechanical model of a DFIG-WT oriented to primary frequency control studies that has been developed by the authors in a previous work [16]. The relationship between input and output variables of each of the subsystems of the model are summarized in the set of equations (1), where: *T*, *P*, and ω represent torque, power and angular speed; subscripts *g* and *t* are used to indicate the variables referring to the generator and the turbine; subscript base is used to denote the per-unit system base values of the different variables; and f_s, *p*, and *n* are the grid frequency, the number of pole pairs of the DFIG and the gear-box ratio, respectively.

$$\begin{aligned} \omega_{g,\mathrm{base[rad/s]}} &= 2\pi f_{s[\mathrm{Hz}]}/p = \omega_{g[\mathrm{rad/s}]}/\omega_{g[\mathrm{pu}]} \\ \omega_{t,\mathrm{base[rad/s]}} &= 2\pi f_{s[\mathrm{Hz}]}/(p.n) = \omega_{t[\mathrm{rad/s}]}/\omega_{t[\mathrm{pu}]} \\ T_{g,\mathrm{base}[N\cdot\mathrm{m}]} &= P_{\mathrm{base}[W]}/\omega_{g,\mathrm{base[rad/s]}} = T_{g[N\cdot\mathrm{m}]}/T_{g[\mathrm{pu}]} \\ T_{t,\mathrm{base}[N\cdot\mathrm{m}]} &= P_{\mathrm{base}[W]}/\omega_{t,\mathrm{base[rad/s]}} = T_{t[N\cdot\mathrm{m}]}/T_{t[\mathrm{pu}]} \end{aligned} \quad (1)$$

Equations (2)–(6) represent the dynamics of the wind turbine [17], [18], where ρ, *R*, *v*, C_p, λ, and β are the air density, the rotor radius, the wind speed, the power coefficient, the tip speed ratio and the blade pitch angle, respectively. The terms K_p and K_λ are the power and speed constants, respectively, and they depend on the constructive characteristics of the wind turbine. A "one mass" system has been considered to represent the rotational dynamics of the gear-box, the wind turbine and the electrical generator [19], [20] whose equivalent moment of inertia is J_{eq}.

$$\begin{aligned} P_{t[pu]} &= P_{t[W]}/P_{\mathrm{base}[W]} \\ &= \left(0.5\rho\pi R^2/P_{\mathrm{base}}\right) v^3 C_p\left(\lambda,\beta\right) \\ &= K_p v^3 C_p\left(\lambda,\beta\right) \end{aligned} \quad (2)$$

$$\begin{aligned} \lambda &= \omega_{t[\mathrm{pu}]}\omega_{t,\mathrm{base}[rad/s]} R_{[m]}/v_{[\mathrm{m/s}]} \\ &= K_\lambda \omega_{t[\mathrm{pu}]}/v_{[\mathrm{m/s}]} \end{aligned} \quad (3)$$

$$\begin{aligned} C_p\left(\lambda,\beta\right) &= P_t/P_{\mathrm{wind}} \\ &= \mathrm{c}_1\left(\mathrm{c}_2/\lambda_i - \mathrm{c}_3\beta - \mathrm{c}_4\right) e^{-\mathrm{c}_5/\lambda_i} + \mathrm{c}_6\lambda \end{aligned} \quad (4)$$

$$1/\lambda_i = \left(\lambda + 0.08\beta\right)^{-1} - 0.035\left(\beta^3+1\right)^{-1} \quad (5)$$

$$T_{t[\mathrm{pu}]} = P_{t[\mathrm{pu}]}/\omega_{t[\mathrm{pu}]} \quad (6)$$

Both the DFIG and the RSC have been considered as a single first-order dynamics actuator [20]–[22], with a time constant τ_{C}, whose input is the electromagnetic reference torque from the speed control system, T_{em}^*. Finally, the function of the pitch angle controller is to limit the power captured by the turbine to avoid the rotor acceleration under high wind speed conditions [23].

To ensure an optimal extraction of wind power by the turbine, the speed controller in a DFIG-WT uses a MPPT characteristic (Fig. 3) that can be represented by equation (7), where K_{opt} is the optimization constant, whose value depends on the type of turbine. With respect to Fig. 3, the segment A-B corresponds to the starting zone. In segment B-C, known as optimization zone, the control system modifies the rotor speed by regulating both the amplitude and the frequency of the current injected into the DFIG rotor to adjust its operation to the maximum power points. Finally, in segment C-D, the speed is kept almost constant until the power reaches its rated value. When the rotor speed goes beyond point D, the control actions are carried out by the pitch angle controller.

$$P_t = \begin{cases} \dfrac{K_{\mathrm{opt}}{\omega_0}^3}{\left(\omega_0 - \omega_{\min}\right)}\left(\omega_g - \omega_{\min}\right), & \omega_{\min} \le \omega_g < \omega_0 \\ K_{\mathrm{opt}}{\omega_g}^3, & \omega_0 \le \omega_g \le \omega_1 \\ \dfrac{\left(P_{\max} - K_{\mathrm{opt}}{\omega_1}^3\right)}{\left(\omega_{\max} - \omega_1\right)}\left(\omega_g - \omega_{\max}\right) + P_{\max}, & \omega_1 < \omega_g \le \omega_{\max} \end{cases} \quad (7)$$

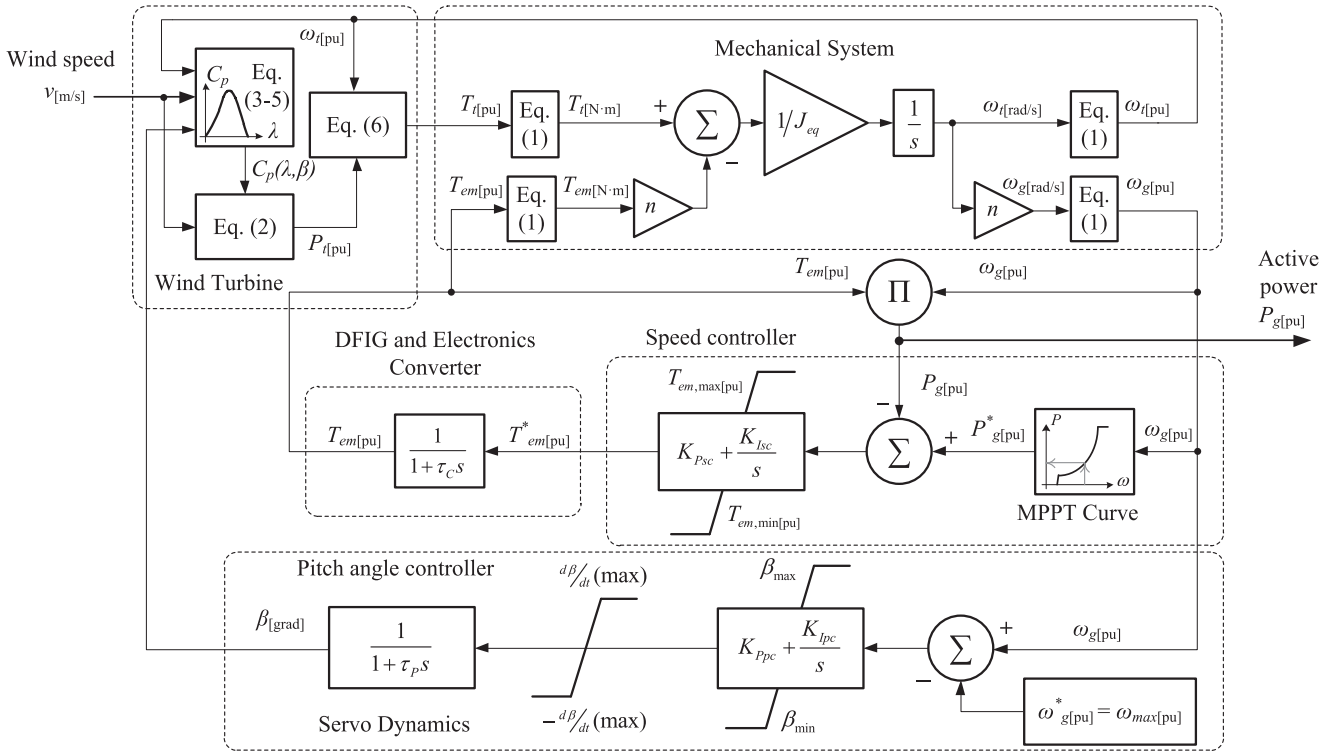

Fig. 2. Block diagram of a simplified model of a DFIG-based wind turbine.

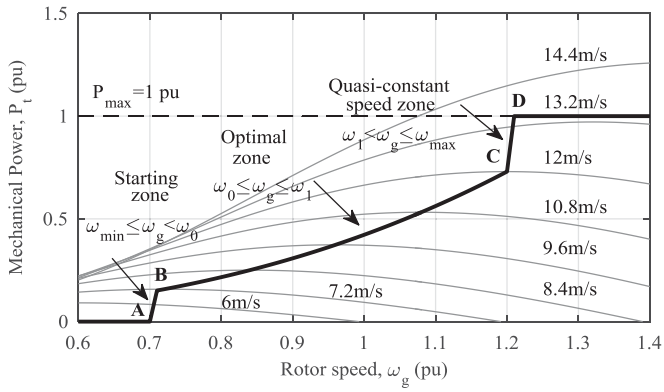

Fig. 3. MPPT-curve implemented.

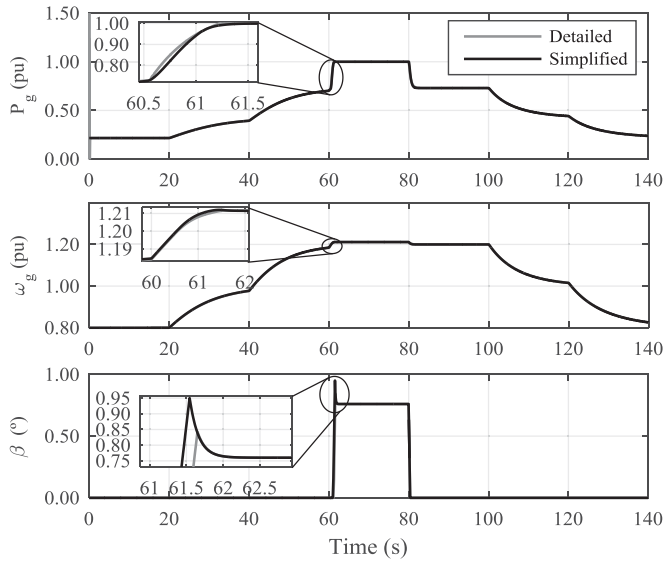

Fig. 4. DFIG-WT simplified model vs. MATLAB/Simulink detailed model.

To show the validity of the proposed model, it has been compared to the DFIG-WT model available in the MATLAB/Simulink library with its power losses disabled, a much more detailed model, although impractical for large scale power systems studies. A stepped wind speed profile (from 8 to 14 m/s with an increasing rate of 2 m/s each 20 seconds, and then, from 14 to 8 m/s with a similar decreasing rate) has been considered as an input for the two models. Fig. 4 illustrates the behavior of the most relevant variables of the DFIG-WT for a power-frequency analysis: the total active power generated, P_g, ω_g, and β. The results show the accuracy of the proposed model in terms of the transient and steady-state response despite all the approximations considered. There is a minimum time delay between the compared models, representing less than 3% of the DFIG-WT inertia constant.

III. Virtual Inertia of a DFIG-Based Wind Turbine

The frequency dynamic behavior of a power system in a situation of imbalance between generation and demand is determined by the inertial response of the online conventional synchronous generators, by means of the natural interchange of kinetic

energy with the grid. A DFIG-WT lacks this characteristic due to its asynchronous operation and the decoupling between the rotor speed and the grid frequency, thus causing a decrease in the power system stability margin, especially when the participation of such technology becomes important [24], [25]. However, wind turbines do have a significant amount of inertial resources that could be exploited for the benefit of the power system by making some modifications to the existing control systems. In this section, the term "virtual inertia" is introduced to refer to this non-natural response of a DFIG-WT.

The stored kinetic energy variation of a DFIG-WT, when the rotor speed changes from ω_{r0} to ω_{r1}, can be calculated using (8), where: $\Delta\omega_r = \omega_{r1} - \omega_{r0}$, and $J_{\rm eq}$ is the natural moment of inertia.

$$\begin{aligned}\Delta E_{\mathrm{WT}[J]} &= 0.5 J_{eq[kg\cdot m^2]}\left({\omega_{r1}}^2_{[\mathrm{rad/s}]} - {\omega_{r0}}^2_{[\mathrm{rad/s}]}\right)\\ \Delta E_{\mathrm{WT}[J]} &= 0.5 J_{\mathrm{eq}}\left[\left(\omega_{r0}+\Delta\omega_r\right)^2 - {\omega_{r0}}^2\right]\end{aligned} \tag{8}$$

Equation (9) can be obtained by considering the DFIG-WT as if it were a synchronous generator whose rotor speed changes from its synchronism condition, ω_s, to ω_{s1}, where: $\Delta\omega_s = \omega_{s1} - \omega_s$ and $J_{\rm vir}$ is the virtual moment of inertia.

$$\begin{aligned}\Delta E_{\mathrm{WT}} &= 0.5 J_{\mathrm{vir}}\left({\omega_{s1}}^2 - {\omega_s}^2\right)\\ &= 0.5 J_{\mathrm{vir}}\left[\left(\omega_s+\Delta\omega_s\right)^2 - {\omega_s}^2\right]\end{aligned} \tag{9}$$

By matching (8) and (9), the virtual moment of inertia of a DFIG-WT can be defined as:

$$J_{\mathrm{vir}} = \frac{\left(2\omega_{r0}+\Delta\omega_r\right)\Delta\omega_r}{\left(2\omega_s+\Delta\omega_s\right)\Delta\omega_s} J_{\mathrm{eq}} \tag{10}$$

In frequency stability studies, it is common to assume the presence of small disturbances, therefore, in (10), typically: $2\omega_{r0} >> \Delta\omega_r$ and $2\omega_s >> \Delta\omega_s$, making it possible to obtain (11), in which the ratio $\Delta\omega_r/\Delta\omega_s$ is defined as the virtual inertia coefficient, k_{vir}.

$$J_{\mathrm{vir}} \approx \frac{\omega_{r0}\Delta\omega_r}{\omega_s\Delta\omega_s} J_{\mathrm{eq}} = \frac{\omega_{r0}}{\omega_s} k_{\mathrm{vir}} J_{\mathrm{eq}} \tag{11}$$

From (11), it is possible to conclude that the virtual inertia of a DFIG-WT not only depends on its natural inertia, but also on the rotor speed before the disturbance, ω_{r0}, and the virtual inertia coefficient. In contrast to a synchronous generator, in which its rotor speed, ω_s, is determined by the grid frequency and therefore varies slightly, the variation of the rotor speed in a DFIG-WT may be much greater, thus, its virtual inertia could exceed the natural inertia. However, it is important to keep in mind that J_{vir} corresponds to an instantaneous value, with a transient nature and relatively short duration.

IV. Shifting the MPPT Curve to Emulate an Inertial Response in a DFIG-Based Wind Turbine

The previous section showed that, for a DFIG-WT, it is possible to emulate an inertial response to support the grid frequency by making use of its kinetic energy. In this paper, the optimized power point tracking (OPPT) method presented in [14] has been adapted for a suitable implementation in a DFIG-WT and extended for allowing an adequate performance under actual frequency variations. An additional derivative of frequency feature applied to the OPPT method is also proposed in order to contribute to reducing the rate of change of frequency (ROCOF) of the grid.

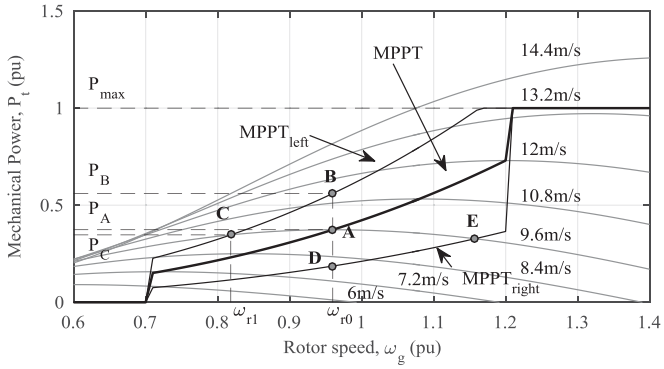

Fig. 5. Shifting the MPPT-curve by OPPT method.

A. Optimal Power Point Tracking method

To explain the principle of this method, let us assume that the DFIG-WT is subject to a constant wind speed, and that, initially, its operation is governed by the implemented MPPT curve as shown in Fig. 5. If an under-frequency event occurs (e.g., due to a sudden loss of certain generating units), conventional power plants are required to increase their production using the available primary energy reserves and trying to reduce the generation-demand power imbalance. To enable the DFIG-WT participation in the resolution of this contingency, it should be able to increase the active power injected into the grid, i.e., to go from its stable operation condition, at point A, to point B, immediately. This is achieved by shifting the MPPT curve to the left. Note that the requested active power, P_B, exceeds the mechanical power given by the turbine, causing the rotor deceleration $(\omega_{r0} \rightarrow \omega_{r1})$ until both powers equilibrate again at point C. It should be noted that, throughout this process (A–B–C), the DFIG-WT has given part of its stored kinetic energy to reduce the rate of change of the grid frequency. However, from this point on, it works in a sub-optimal condition (point C), which is not technically and economically desirable $(P_C < P_A)$. Therefore, after providing frequency support, it is necessary that the reference signal of the active power recovers its optimum value, P_A. Similarly, in an over-frequency scenario, the inertial response of a DFIG-WT would have to describe the path (A–D–E) and, finally, return to the optimum point A.

The MPPT curve can be shifted to the left or right, by modifying the value of K_{opt} from (7). If this constant is multiplied by a factor whose value depends on the grid frequency changes, f_{kopt}, the parameter K_{OPPT} is obtained. To obtain the relationship between K_{OPPT} and K_{opt}, given by f_{kopt}, it is reasonable to consider that, in the fast-frequency response stage (A–B–C), the optimal and sub-optimal active power values, P_A and P_C, are approximately equal, particularly when considering small disturbances. Equation (12) can be obtained by applying this

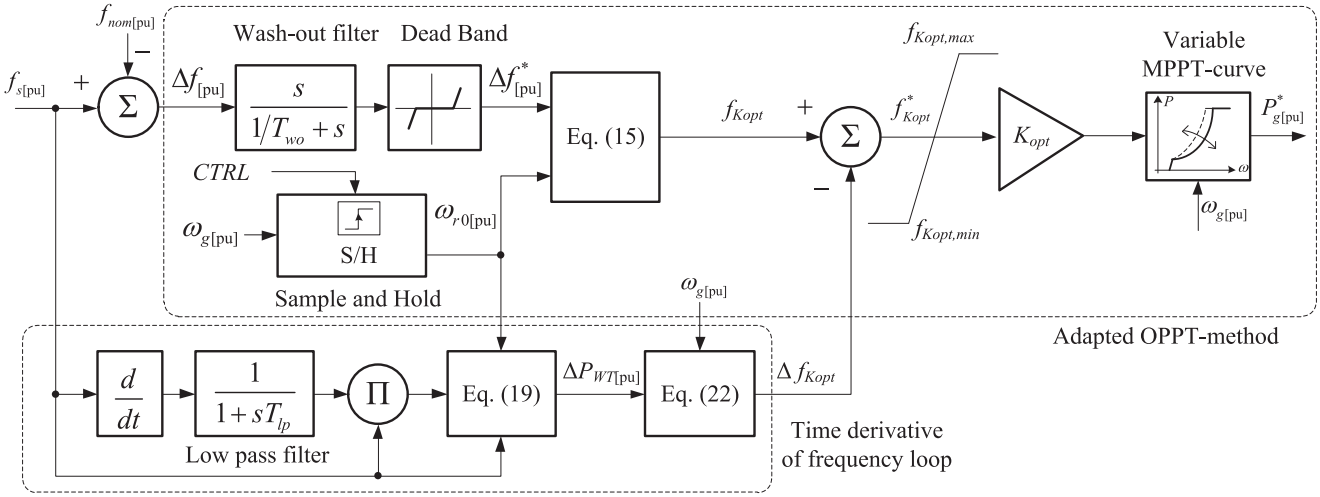

Fig. 6. Control scheme for implementing the proposed method.

approximation to the term corresponding to the optimization zone in (7).

$$K_{\mathrm{OPPT}}\omega_{r1}^3 \approx K_{\mathrm{opt}}\omega_{r0}^3 \tag{12}$$

Expressing ω_{r1} in terms of the rotor speed deviation, $\Delta\omega_r = \omega_{r1} - \omega_{r0}$, and the virtual inertia coefficient, k_{vir}, defined in (11):

$$\omega_{r1} = \omega_{r0} + \Delta\omega_r = \omega_{r0} + k_{\mathrm{vir}}\Delta\omega_s \tag{13}$$

Substituting (13) into (12), K_{OPPT} can be expressed by (14), which coincides with the expression provided by [14].

$$K_{\mathrm{OPPT}} = \frac{{\omega_{r0}}^3}{\left(\omega_{r0} + k_{\mathrm{vir}}\Delta\omega_s\right)^3}K_{\mathrm{opt}} = f_{\mathrm{kopt}}K_{\mathrm{opt}} \tag{14}$$

Finally, making $\Delta\omega_s = 2\pi\Delta f/p$, the virtual inertia factor, f_{kopt}, is defined as:

$$f_{\mathrm{kopt}} = \frac{\omega_{r0[\mathrm{rad/s}]}^3}{\left(\omega_{r0[\mathrm{rad/s}]} + 2\pi k_{\mathrm{vir}}\Delta f_{[\mathrm{Hz}]}/p\right)^3} \tag{15}$$

Fig. 6 shows the scheme that should be added to the DFIG-WT speed controller (Fig. 2) to implement the proposed control strategy. The subsystem of the upper part of Fig. 6, receives the rotor speed, ω_g, and the grid frequency deviation, Δf, as inputs. Δf is passed through a first-order high pass filter (with time constant, T_{wo}) to remove the residual component of the quasi-steady state frequency deviation produced by the actions of primary regulation in the power system. A dead-band block has also been added to provide the controller with a certain level of insensitivity to frequency variations. When a frequency deviation is detected ($\Delta f^* \neq 0$), the adapted OPPT controller sends a binary control signal, *CTRL*, to a Sample and Hold routine in order to store the pre-disturbance rotor speed, ω_{r0}, and to guarantee the continuous evaluation of (15) to find f_{kopt}. This allows an adequate implementation of the OPPT method in case of real frequency fluctuations, caused by sudden load changes, intermittent wind power injection, etc. By multiplying f_{kopt} and K_{opt}, it is possible to modify the MPPT curve and, consequently, the active power reference of the DFIG-WT speed controller. The bounds $f_{\mathrm{Kopt,max}}$ and $f_{\mathrm{Kopt,min}}$ have been assigned to limit the shift of the MPPT curve within a stable operating margin.

B. Sensitivity to the time derivative of frequency

In order to develop the desired extension of the OPPT method, it is necessary to find a relationship between the active power increase/decrease requirement of a DFIG-WT and the time derivative of the grid frequency. Based on the concept of virtual inertia explained in section III, the kinetic energy stored in the rotating masses of the DFIG-WT can be calculated as:

$$E_{\mathrm{WT}[J]} = 0.5J_{\mathrm{vir}[\mathrm{kg\cdot m^2}]}\omega_{\mathrm{s}[\mathrm{rad/s}]}^2 \tag{16}$$

By considering the time derivative of (16), it is possible to evaluate the power delivered by the DFIG-WT due to a change in the rotor speed:

$$\begin{aligned}\Delta P_{\mathrm{WT}[W]} &= \frac{dE_{\mathrm{WT}[J]}}{dt} = 0.5J_{\mathrm{vir}[\mathrm{kg\cdot m^2}]}\frac{d\omega_{\mathrm{s}[\mathrm{rad/s}]}^2}{dt} \\ &= J_{\mathrm{vir}[\mathrm{kg\cdot m^2}]}\omega_{s[\mathrm{rad/s}]}\frac{d\omega_{s[\mathrm{rad/s}]}}{dt}\end{aligned} \tag{17}$$

Using the definition of inertia constant ($H = 0.5J\omega^2/P_{\mathrm{base}}$) and a per unit system, it is possible to express (17) in terms of the virtual inertia constant, H_{vir}, as follows:

$$\Delta P_{\mathrm{WT[pu]}} = \frac{\Delta P_{\mathrm{WT}[W]}}{P_{\mathrm{base}[W]}} = 2H_{\mathrm{vir}[s]}\omega_{s[\mathrm{pu}]}\frac{d\omega_{s[\mathrm{pu}]}}{dt} \tag{18}$$

Then, by deriving H_{vir} from (11) and making $\omega_{s[\mathrm{pu}]} = f_{s[\mathrm{pu}]}$, equation (18) can be rewritten as:

$$\Delta P_{\mathrm{WT[pu]}} = 2\left(\frac{\omega_{r0[\mathrm{pu}]}}{\omega_{s[\mathrm{pu}]}}k_{\mathrm{vir}}H_{\mathrm{eq}[s]}\right)f_{s[\mathrm{pu}]}\frac{df_{s[\mathrm{pu}]}}{dt} \tag{19}$$

Respecting the MPPT-shifting philosophy, the increment in the active power reference represented by (19), is obtained by acting on f_{kopt} as it can be observed in the subsystem of the lower part of Fig. 6. In this diagram, Δf_{kopt} represents the

deviation of the virtual inertia factor which can be expressed in terms of ΔP_{WT} as:

$$\Delta f_{\mathrm{kopt}} = \frac{\Delta P_{\mathrm{WT[pu]}}}{K_{\mathrm{opt}}\omega^3_{g[\mathrm{pu}]}} \tag{20}$$

However, the direct application of (20) for calculating f^*_{kopt} in Fig. 6 does not take into account the amount of the kinetic energy available in the wind turbine, and the control actions provided by the time derivative of frequency loop are dominant over the ones provided by the adapted OPPT method. In order to obtain a better coordination of both contributions, a weighting factor, W_{vir}, has been introduced, defined as the ratio of the releasable kinetic energy in per unit respect to the maximum:

$$W_{\mathrm{vir}} = \frac{\omega_g^2 - \omega^2_{\mathrm{min}}}{\omega^2_{\mathrm{max}} - \omega^2_{\mathrm{min}}} \tag{21}$$

Thus, the Δf_{kopt} to be used in the control scheme (Fig. 6) is redefined as:

$$\Delta f_{\mathrm{kopt}} = \frac{\Delta P_{\mathrm{WT[pu]}}}{K_{\mathrm{opt}}\omega^3_{g[\mathrm{pu}]}} W_{\mathrm{vir}} \tag{22}$$

A first-order low pass filter (with time constant, T_{lp}) has been added in order to remove the measurement noise from the derivative of frequency.

When a frequency event occurs, a coordinated operation of the two subsystems that make up the proposed method (Fig. 6) is expected. In the initial stage of a frequency event, the term Δf_{kopt} is dominant because *df/dt* has a large value that will decline as the grid frequency reaches its maximum instantaneous deviation. At this point, the effect of the control action, f_{kopt}, provided by the adapted OPPT method will have reached its maximum value, because it has been conceived to respond to any change in Δf. Finally, in the frequency rebound stage, the term f_{kopt} is able to compensate the sign change of *df/dt*, and mitigate the power system frequency fluctuations as it will be shown in section VI.

V. Participation of DFIG-Based Wind Turbine in Primary Frequency Control

As discussed in previous sections, it is expected that the frequency support provided by the DFIG-WT covers the first seconds after the disturbance. According to the structure of the ancillary services in a power system, such period corresponds to primary frequency regulation [26]. In this sense, the proposed DFIG-WT model has been incorporated into a traditional primary frequency control scheme for a single control area (Fig. 7) based on [27], [28].

For this study, four conventional generation technologies have been considered: hydro and thermal plants based on coal, nuclear energy and combined-cycle. All these models are taken from [27], [29]–[33], and the values of the most significant parameters are summarized in the Appendix. The equivalent power system inertia constant, H_{T}, is determined by (23), where H_{i} and w_i are the inertia constant and the participation factor from each power plant, respectively, and *m* is the number of online conventional power plants.

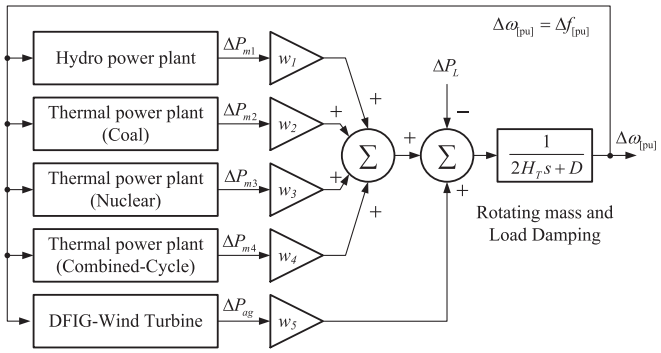

Fig. 7. Primary frequency control scheme.

TABLE I
Inertia Constant and Participation Index

Type of power plant	H_i (s)	w_{i} (%)[a]
Hydro	3.6	5
Coal	3	15
Nuclear	7	35
Combined-Cycle	6.5	15
Wind	–	30

[a]Approximate percentages based on the actual power demand coverage data in the SPPS on 06/04/2015 at 04:00 (UTC +01:00) [34].

$$H_T = \sum_{i=1}^{m} H_i \cdot w_i \tag{23}$$

VI. Simulation and Results

In this section, MATLAB/Simulink time-domain simulations have been carried out in order to study the impact of the inertial contribution from a DFIG-WT on the power system dynamics. To illustrate the method, the Spanish Peninsular Power System (SPPS) has been considered in a low demand scenario (18 552 MW) [34]. It has been assumed that all the wind power plants connected to the SPPS are composed of DFIG-WTs and subject to a common wind speed (9.6 m/s), that is kept constant during the simulation. The participation index on the coverage of the demand for each type of power plant considered, along with their inertia constant, are summarized in Table I [27], [35]. According to [26], the load damping for this system is 1%/Hz ($D = 0.5$ pu). In addition, the integral characteristic of all the conventional plant speed governors has been disabled in order to better show the behavior of the proposed method, particularly, to assess the ability of the technique for recovering the pre-disturbance operating point after providing frequency support, independently of the capability of the rest of the plants for reducing the quasi-steady frequency error.

A. Sudden load increase

Firstly, a sudden load increase of 600 MW ($\Delta P_L = 0.03$ pu) is introduced in the power system in order to generate an

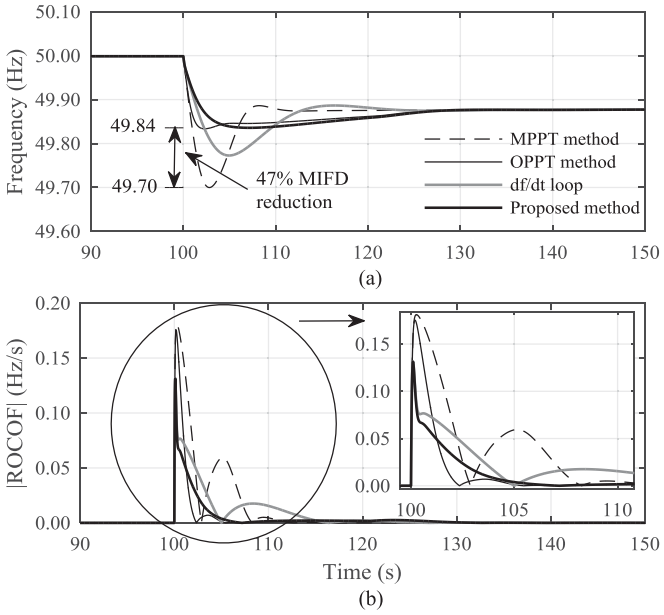

Fig. 8. Behavior of the grid frequency during a sudden load increase.

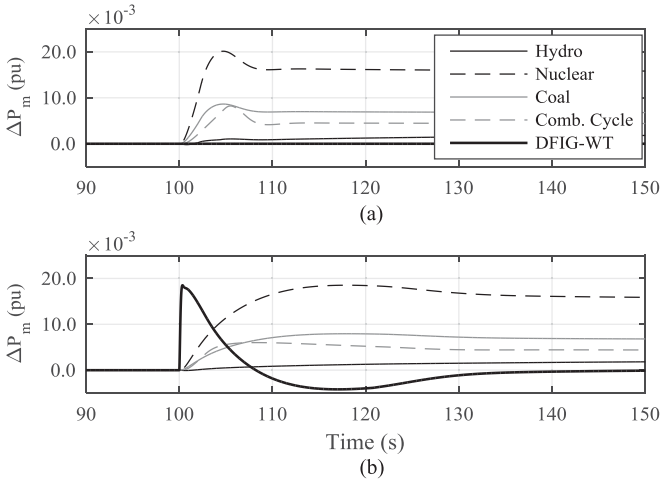

Fig. 9. Primary frequency control provided by each power plant during a sudden load increase: a) Without DFIG-WT frequency response, b) With the DFIG-WT frequency response.

under-frequency event (after 100 s from the beginning of the simulation). In Fig. 8, the dynamic behavior of the power system frequency and the ROCOF is shown in four cases: with the conventional MPPT control, with the inertial support provided only by the adapted OPPT method, with the fast-frequency response provided exclusively by the time derivative of frequency loop, and with the combined action of the proposed extended OPPT method. It is evident that, by means of controlled inertial response, the DFIG-WTs help to significantly reduce the maximum instantaneous frequency deviation (MIFD), thus improving the power system stability margin. Such reduction results in a slower action of the speed governors of conventional power plants (Fig. 9) and, therefore, the power system frequency reaches its quasi-steady state in a slightly longer time. Note in

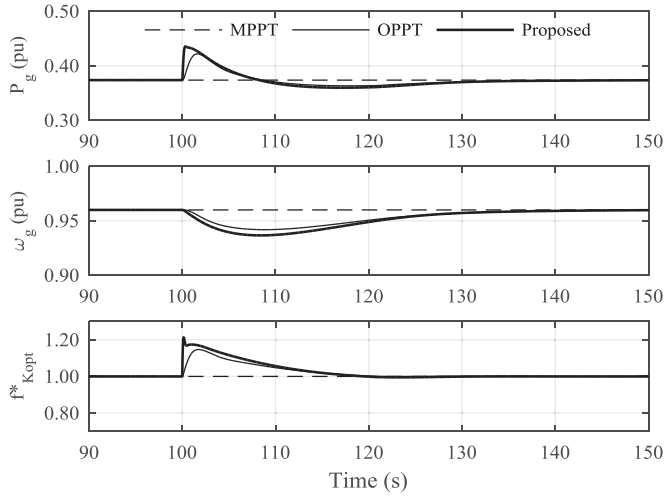

Fig. 10. DFIG-WT response during a sudden load increase.

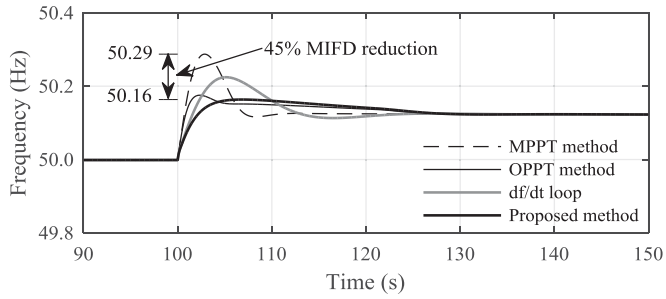

Fig. 11. Behavior of the grid frequency during a sudden load decrease.

Fig. 8(b) that the ROCOF is better reduced by applying the proposed extension of the OPPT method.

Figure 10 shows the behavior of certain variables of the DFIG-WT during this contingency. Normally, the f^*_{kopt} factor –that combines the control signals f_{kopt} and Δf_{kopt}– has a unit value, which means that both the active power, P_g, and the rotor speed, ω_{g}, are operating at their optimum values according to the MPPT characteristic. Note that, from the instant in which the disturbance is introduced, the DFIG-WT rapidly increases P_g for providing fast-frequency response. According to the reasoning in Section IV, the rotor speed will begin to decrease until a new sub-optimal operation point is reached. After this transient frequency support, f^*_{kopt} will gradually recover its optimum value and it will lead P_g and ω_g to recover their pre-disturbance values.

B. Sudden load decrease

A complementary test is carried out in which the power system is subjected to a sudden load decrease of 600 MW ($\Delta P_L = -0.03$ pu) so that it causes an over-frequency event. Figures 11 and 12 illustrate the transient behavior of the grid frequency and the DFIG-WT dynamic response, respectively, showing almost symmetrical results.

Fig. 13 summarizes the reduction of the MIFD achieved by the participation of the DFIG-WTs in the grid frequency support

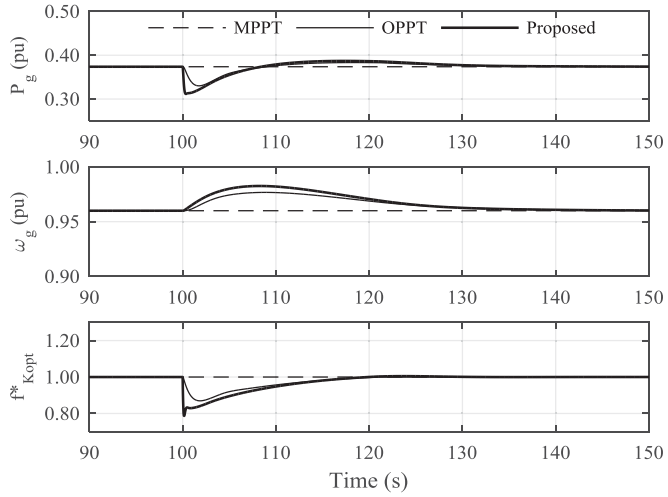

Fig. 12. DFIG-WT response during a sudden load decrease.

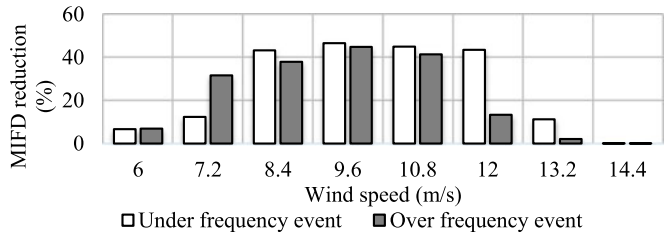

Fig. 13. Reduction of the MIFD according to wind speed.

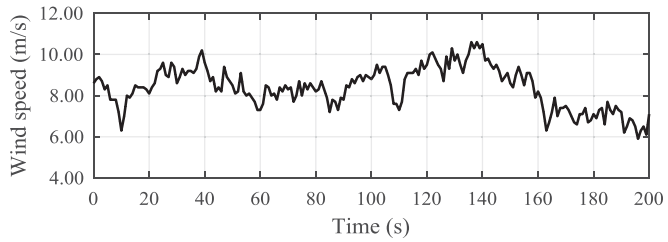

Fig. 14. Real wind speed profile.

under different wind conditions. It can be seen that the inertial response is strongly influenced by the incident wind speed. Its impact is much greater for operation points within the optimization zone of the MPPT curve (segment B-C in Fig. 3), since the OPPT method is conceived for maintaining the DFIG-WT operation within stable and secure limits, both angular rotor speed and output active power.

C. Real wind speed conditions

Finally, in order to assess the operation of the DFIG-WT with the extended OPPT method under real wind conditions, the system of Fig. 7 is tested with a constant power demand ($\Delta P_L = 0$ pu) and the DFIG-WT subjected to the wind speed profile shown in Fig. 14. The consequent intermittent wind power injection introduces undesirable grid frequency fluctuations.

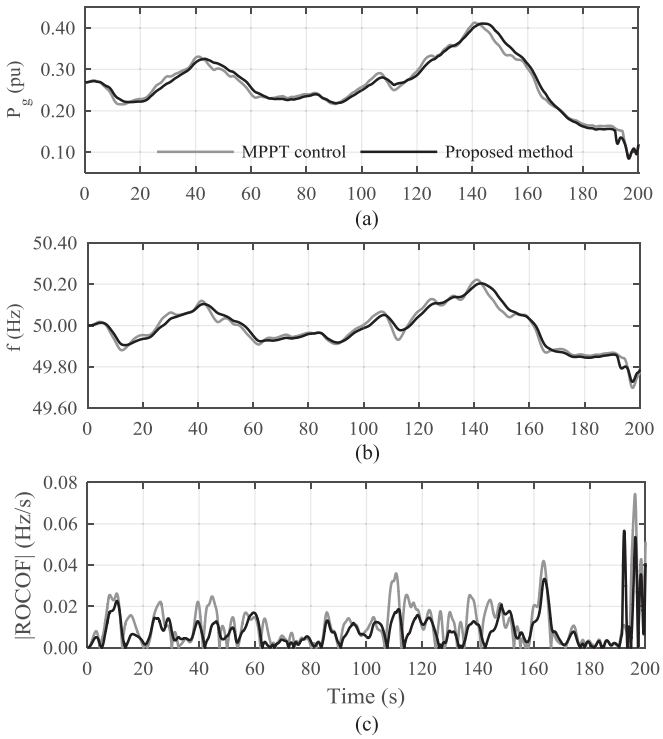

Fig. 15. Behavior of the DFIG-WT and power system variables under real wind speed conditions.

The continuous application of the proposed method provides for the additional feature of power smoothing, which can be seen in Fig. 15(a), leading to the partial mitigation of frequency oscillations shown in Fig. 15(b). Fig. 15(c) compares the rate of change of frequency (ROCOF), showing an average reduction of 24% over the period considered.

VII. Conclusion

This paper presents a simplified model of a DFIG-WT intended for primary frequency regulation studies in large-scale power systems. The model includes an additional control system that allows the DFIG-WT to provide fast-frequency response to the grid in presence of disturbances. The model has been integrated into a traditional primary frequency control scheme to assess its impact on the power system dynamics. The time domain simulations have shown that the inertial contribution of the DFIG-WT by means of the proposed control strategy improves the frequency response of the power system, to a greater or lesser degree depending on the wind conditions. The continuous application of the extended OPPT method under real wind conditions allows the smoothing of the DFIG-WT output power, which results in a reduction of the grid frequency fluctuations.

The technique presented in the paper is suitable for integration of DFIG-WT into large scale power systems. Additional research is needed to assess its validity for weak networks, in which the magnitude of frequency deviations is larger and where the contribution to frequency support can be even more important.

APPENDIX

A. DFIG-WT parameters

TABLE A1
DFIG-BASED WIND TURBINE PARAMETERS

Parameter	Symbol	Value and Units
Base power	$P_{\rm base}$	1.5 MW
Max. /Min. power of the generator	$P_{g,\max}/P_{g,\min}$	1/0.04 pu
Max./Min. torque of the generator	$T_{em.\max}/T_{\rm em.min}$	0.826/0.057 pu
Wind speed at $P_{\rm g} = 0.73$ pu	v_{nom}	12 m/s
Number of pole pairs	p	2
Nominal frequency	$f_{\rm nom}$	50 Hz
Base speed of the turbine	$\omega_{t,\rm base}$	1.644 rad/s
Base speed of the generator	$\omega_{g,\rm base}$	157.08 rad/s
Air density	ρ	1.225 kg/m^3
Radius of the rotor	R	38.5 m
Power constant	K_p	1.901×10^{-3} (m/s)$^{-3}$
Speed constant	K_λ	63.29 m/s
Min. /Max. blade pitch angle	$\beta_{\min}/\beta_{\max}$	0°/45°
Maximum blade pitch angle rate	$(d\beta/dt)$max	2°/s
Turbine-generator inertia constant	$H_{\rm eq}$	5.29 s
DFIG-PEC time constant	τ_C	20 ms
Blade pitch servo time constant	τ_P	0 s
Pitch controller gains	$K_{P\rm pc}/K_{I\rm pc}$	500/0
Speed controller gains	$K_{P\rm sc}/K_{I\rm sc}$	0.3/8

B. MPPT-curve parameters

$K_{\rm opt} = 0.4225,\ {\rm c}_1 = 0.5176,\ {\rm c}_2 = 116,\ {\rm c}_3 = 0.4,\ {\rm c}_4 = 5,\ {\rm c}_5 = 21,\ {\rm c}_6 = 0.0068,\ \omega_{\min} = 0.7$ pu, $\omega_0 = 0.71$ pu, $\omega_1 = 1.2$ pu, $\omega_{\max} = 1.21$ pu.

C. OPPT-method parameters

Dead band = 10 mHz, $k_{\rm vir} = 8$, $f_{\rm Kopt,max} = 1.6$, $f_{\rm Kopt,min} = 0.4$, $T_{\rm wo} = 10$ s, $T_{\rm lp} = 100$ ms.

D. Conventional generation units parameters

TABLE A2
GENERATION UNITS PARAMETERS

	Value and Units		
Parameter	Hydro	Thermal	Comb. Cycle
Deadband	10 mHz	10 mHz	10 mHz
Droop	5%	5%	5%
Main servo time constant	0.2 s	0.2 s	0.2 s
Maximum output power increase/decrease	10%	10%	10%
Maximum gate opening rate	0.16 pu/s	0.05 pu/s	0.02 pu/s
Maximum gate closing rate	−0.16 pu/s	−0.1 pu/s	−0.02 pu/s
Water time constant	1 s		
Temporary droop	0.4 pu		
Reset time	5 s		
Fraction of total turbine power generated by high pressure		0.3	
Reheater time constant		7 s (Coal) 5 s (Nuclear)	
Time constant of main inlet columes and steam chest		0.3 s	
Gate time constant			0.3 s
Gas feeder time constant			7 s
Compressor discharge time constant			0.3 s

REFERENCES

[1] J. MacDowell, S. Dutta, M. Richwine, S. Achilles, and N. Miller, "Serving the Future: Advanced wind generation technology supports ancillary services," *IEEE Power Energy Mag*., vol. 13, no. 6, pp. 22–30, Nov. 2015.

[2] J. Xu *et al.*, "An isolated industrial power system driven by Wind-Coal power for aluminum productions: A case study of frequency control," *IEEE Trans. Power Syst.*, vol. 30, no. 1, pp. 471–483, Jan. 2015.

[3] L. Sigrist, I. Egido, E. L. Miguélez, and L. Rouco, "Sizing and controller setting of ultracapacitors for frequency stability enhancement of small isolated power systems," *IEEE Trans. Power Syst.*, vol. 30, no. 4, pp. 2130–2138, Jul. 2015.

[4] M. Mohseni and S. Islam, "A space vector-based current controller for doubly fed induction generators," presented at the 35th Annu. Conf. IEEE Ind. Electron., Porto, Portugal, 2009, pp. 3868–3873.

[5] M. Liserre, R. Cardenas, M. Molinas, and J. Rodriguez, "Overview of Multi-MW wind turbines and wind parks," *IEEE Trans. Ind. Electron.*, vol. 58, no. 4, pp. 1081–1095, Apr. 2011.

[6] Y.-W. Shen, D.-P. Ke, Y.-Z. Sun, D. S. Kirschen, W. Qiao, and X.-T. Deng, "Advanced auxiliary control of an energy storage device for transient voltage support of a doubly fed induction generator," *IEEE Trans. Sustain. Energy*, vol. 7, no. 1, pp. 63–76, Jan. 2016.

[7] Y. Li, D. Wang, C. Guo, and Y. Li, "Research on DFIGs' participation in frequency regulation and penetration ratio of wind power integration," in *Proc. 2014 Int. Conf. Power Syst. Technol.*, 2014, pp. 2700–2705.

[8] D. Raoofsheibani, E. Abbasi, and K. Pfeiffer, "Provision of primary control reserve by DFIG-based wind farms in compliance with ENTSO-E frequency grid codes," in *Proc. IEEE PES Innovative Smart Grid Technol., Eur.*, 2014, pp. 1–6.

[9] E. M. G. Rodrigues, A. W. Bizuayehu, and J. P. S. Catalão, "Analysis of requirements in insular grid codes for large-scale integration of renewable generation," in *Proc. 2014 IEEE PES T&D Conf. Expo.*, 2014, pp. 1–5.

[10] Y. Liu, J. R. Gracia, T. J. King, and Y. Liu, "Frequency regulation and oscillation damping contributions of variable-speed wind generators in the U.S. eastern interconnection (EI)," *IEEE Trans. Sustain. Energy*, vol. 6, no. 3, pp. 951–958, Jul. 2015.

[11] L.-R. Chang-Chien, W.-T. Lin, and Y.-C. Yin, "Enhancing frequency response control by dfigs in the high wind penetrated power systems," *IEEE Trans. Power Syst.*, vol. 26, no. 2, pp. 710–718, May 2011.

[12] Z.-S. Zhang, Y.-Z. Sun, J. Lin, and G.-J. Li, "Coordinated frequency regulation by doubly fed induction generator-based wind power plants," *IET Renew. Power Gener.*, vol. 6, no. 1, pp. 38–47, Jan. 2012.

[13] L. Xu, G. Wang, L. Fu, Y. Wu, and Q. Shi, "General average model of D-PMSG and its application with virtual inertia control," in *Proc. 2015 IEEE Int. Conf. Mechatronics Autom.*, 2015, pp. 802–807.

[14] Y. Wang, J. Meng, X. Zhang, and L. Xu, "Control of PMSG-based wind turbines for system inertial response and power oscillation damping," *IEEE Trans. Sustain. Energy*, vol. 6, no. 2, pp. 565–574, Apr. 2015.

[15] T. M. Masaud and P. K. Sen, "Modeling and control of doubly fed induction generator for wind power," in *Proc. 2011 North Amer. Power Symp.*, 2011, pp. 1–8.

[16] D. Ochoa and S. Martinez, "A simplified Electro-Mechanical model of a DFIG-based wind turbine for primary frequency control studies," *IEEE Latin Amer. Trans.*, vol. 14, no. 8, pp. 3614–3620, Aug. 2016.

[17] V. Reyes, J. J. Rodríguez, O. Carranza, and R. Ortega, "Review of mathematical models of both the power coefficient and the torque coefficient in wind turbines," in *Proc. 2015 IEEE 24th Int. Symp. Ind. Electron.*, 2015, pp. 1458–1463.

[18] Y. Xia, K. H. Ahmed, and B. W. Williams, "Wind turbine power coefficient analysis of a new maximum power point tracking technique," *IEEE Trans. Ind. Electron.*, vol. 60, no. 3, pp. 1122–1132, Mar. 2013.

[19] T. Hardy and W. Jewell, "Emulation of a 1.5 MW wind turbine with a DC motor," presented at the IEEE Power and Energy Soc. General Meeting, San Diego, CA, USA, 2011, pp. 1–8.

[20] K. Clark, N. W. Miller, and J. J. Sánchez-Gasca, "Modeling of GE wind turbine-generators for grid studies," Gen. Electr. Int., Inc., Schenectady, NY, USA, vol. 4, 2010.

[21] N. W. Miller, J. J. Sanchez-Gasca, W. W. Price, and R. W. Delmerico, "Dynamic modeling of GE 1.5 and 3.6 MW wind turbine-generators for stability simulations," presented at the IEEE Power Eng. Soc. General Meeting, 2003, pp. 1977–1983.

[22] N. R. Ullah, T. Thiringer, and D. Karlsson, "Temporary Primary Frequency control support by variable speed wind Turbines-Potential and applications," *IEEE Trans. Power Syst.*, vol. 23, no. 2, pp. 601–612, May 2008.

[23] A. B. Attya and T. Hartkopf, "Wind turbine contribution in frequency drop mitigation—Modified operation and estimating released supportive energy," *IET Gener. Transm. Distrib.*, vol. 8, no. 5, pp. 862–872, May 2014.
[24] G. Lalor, A. Mullane, and M. O'Malley, "Frequency control and wind turbine technologies," *IEEE Trans. Power Syst.*, vol. 20, no. 4, pp. 1905–1913, Nov. 2005.
[25] R. Doherty, A. Mullane, G. Nolan, D. J. Burke, A. Bryson, and M. O'Malley, "An assessment of the impact of wind generation on system frequency control," *IEEE Trans. Power Syst.*, vol. 25, no. 1, pp. 452–460, Feb. 2010.
[26] Red Eléctrica de España, "Procedimiento de Operación 1.5." [Online]. Available: http://www.ree.es/es/actividades/operacion-del-sistema-electrico/procedimientos-de-operacion, Accessed on: Feb. 25, 2016 (in Spanish).
[27] P. Kundur, *Power System Stability and Control*, 1st ed. New York, NY, USA: McGraw-Hill, 1994.
[28] A. Gomez-Exposito, A. Conejo, and C. Cañizares, *Electric Energy Systems—Analysis and Operation*, 1st ed. Boca Raton, FL, USA: CRC Press, 2009.
[29] N. Kakimoto and K. Baba, "Performance of gas turbine-based plants during frequency drops," *IEEE Trans. Power Syst.*, vol. 18, no. 3, pp. 1110–1115, Aug. 2003.
[30] G. Lalor, J. Ritchie, D. Flynn, and M. J. O'Malley, "The impact of combined-cycle gas turbine short-term dynamics on frequency control," *IEEE Trans. Power Syst.*, vol. 20, no. 3, pp. 1456–1464, Aug. 2005.
[31] M. R. B. Tavakoli, B. Vahidi, and W. Gawlik, "An educational guide to extract the parameters of heavy duty gas turbines model in dynamic studies based on operational data," *IEEE Trans. Power Syst.*, vol. 24, no. 3, pp. 1366–1374, Aug. 2009.
[32] H. Emam Shalam, M. A. Moustafa Hassan, and A. B. G. Bahgat, "Parameter estimation and dynamic simulation of gas turbine model in combined cycle power plants based on actual operational data," *J. Amer. Sci.*, vol. 7, no. 5, pp. 303–310, 2011.
[33] F. P. de Mello and D. J. Ahner, "Dynamic models for combined cycle plants in power system studies," *IEEE Trans. Power Syst.*, vol. 9, no. 3, pp. 1698–1708, Aug. 1994.
[34] Red Eléctrica de España, "Electricity demand tracking in real time, associated generation mix and CO2 emissions." [Online]. Available: https://demanda.ree.es/demandaEng.html, Accessed on: Feb. 25, 2016.
[35] C. Martinez and V. Casajús, "Mix de generación en el sistema eléctrico español en el horizonte 2030," Foro Nuclear, 2007.

Danny Ochoa (M'15) was born in Ecuador in 1987. He received the B.S. degree in electrical engineering from the Universidad de Cuenca, Cuenca, Ecuador, in 2011 and the M.S. degree in electrical engineering from the Universidad Politecnica de Madrid (UPM), Madrid, Spain, in 2014. He is currently working toward the Ph.D. degree in electrical and electronics engineering at UPM. His research interests are wind energy integration, control, operation, and ancillary services in power systems.

Sergio Martinez (M'02) was born in Spain in 1969. He received the M.S. degree in industrial engineering and the Ph.D. degree in electrical engineering from the Universidad Politecnica de Madrid (UPM), Madrid, Spain, in 1993 and 2001, respectively. He is an Associate Professor with the Department of Electrical Engineering, UPM. His research interests include electrical generation from renewable energy and electrical metrology.